Reprinted from Preprint Volume: Conference on Cloud Physics and Atmospheric Electricity, July 31-August 4, 1978, Issaquah, Wash. Published by The American Meteorological Society, Boston, Mass.

8.3

AIR MOTIONS, MESOSCALE STRUCTURE AND CLOUD MICROPHYSICS ASSOCIATED WITH A COLD FRONT

Peter V. Hobbs, John D. Locatelli, Thomas J. Matejka and Robert A. Houze, Jr.

Atmospheric Sciences Department
University of Washington
Seattle, Washington

1. INTRODUCTION

In this paper we describe the organization, movement and origins of the precipitation associated with a cold front which was well-documented, as part of the CYCLES PROJECT, with the quantitative radar, airborne and ground facilities described by Hobbs (1978).

2. SYNOPTIC SITUATION

On November 17, 1976, a cold front, associated with an occluding cyclonic storm, centered 1200 km to the north, moved east-southeast into Washington State (Fig. 1). The surface frontal passage at the CP-3 radar site (Pt. Brown in Fig. 1) occurred at 0730 PST and was marked by a rise in pressure, a slight drop in temperature, and a shift in the wind from 220° at 9 m s^{-1} to 275° at 6 m s^{-1} within a period of 10 min. The windshift accompanying the frontal passage appeared as a marked line of discontinuity in the Doppler velocity field on the PPI color-displays of the CP-3 radar. This line of discontinuity was used to determine the orientation of the surface front and track its movement across the area covered by the radar.

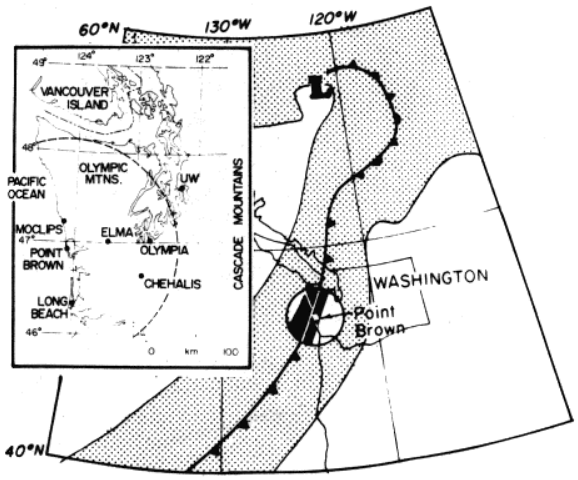

Figure 1. Location of the CP-3 radar at Pt. Brown, Washington, and its area of coverage (circle). Also shown are the cloud shield (light shading), the band of precipitation (dark shading) associated with the front and the surface positions of the front and center of low pressure at 0715 PST on November 17, 1976. The inset shows an expanded view of Western Washington and the locations of the high-resolution precipitation gauges.

3. LARGE AND SMALL MESOSCALE STRUCTURE OF THE PRECIPITATION

The precipitation accompanying the passage of this system through Western Washington consisted of a 50 km wide band of precipitation in the warm sector followed by a large precipitation zone, up to 125 km wide, associated with the cold front. In this paper we are concerned primarily with the sub-structure of the cold-frontal precipitation zone.

The cold-frontal precipitation zone contained five mesoscale bands of heavier rain, from 4 to 50 km in width. Four of these bands (labeled 1-4), as well as the warm-sector band, are shown in Fig. 2(a), and their reflectivities in Fig. 2(b). Although it is not possible in Fig. 2(b) to show all of the internal structure of the bands revealed by the radar, the essence of their internal structures is depicted. The times at which various bands passed over the six high-resolution precipitation gauges (shown in Fig. 1) are indicated in Fig. 2(a). The contribution of these features to the precipitation at each of the gauges is shown in Fig. 3.

A very narrow rainband (about 4 km in width) coincided with the frontal windshift line at the surface. This band (called band 5) is shown in Fig. 4. The effects of band 5 on the precipitation are indicated in Fig. 3, where it can be seen that its passage over Moclips, Pt. Brown and Elma caused noticeable increases in the precipitation rates.

4. MOTIONS OF THE RAINBANDS AND THEIR PRECIPITATION CORES

Previous studies (Browning and Harrold, 1969; Austin and Houze, 1972; Hobbs and Locatelli, 1978) have shown that rainbands in cyclonic storms contain numerous precipitation cores. Bands 1-5 of the cold-frontal band contained precipitation cores which covered horizontal areas from 25 to 300 km^2. These cores could be tracked with the radar for up to 50 min. The precipitation cores in band 5 were distinct from those in the other bands; the cores in band 5 had ellipsoidal shapes with similar orientations and were aligned along the surface cold front (Fig. 5). The precipitation cores in bands 1-4, on the other hand, were irregular in shape and randomly positioned. Other narrow cold-frontal bands which we have studied have similar structures to that of band 5.

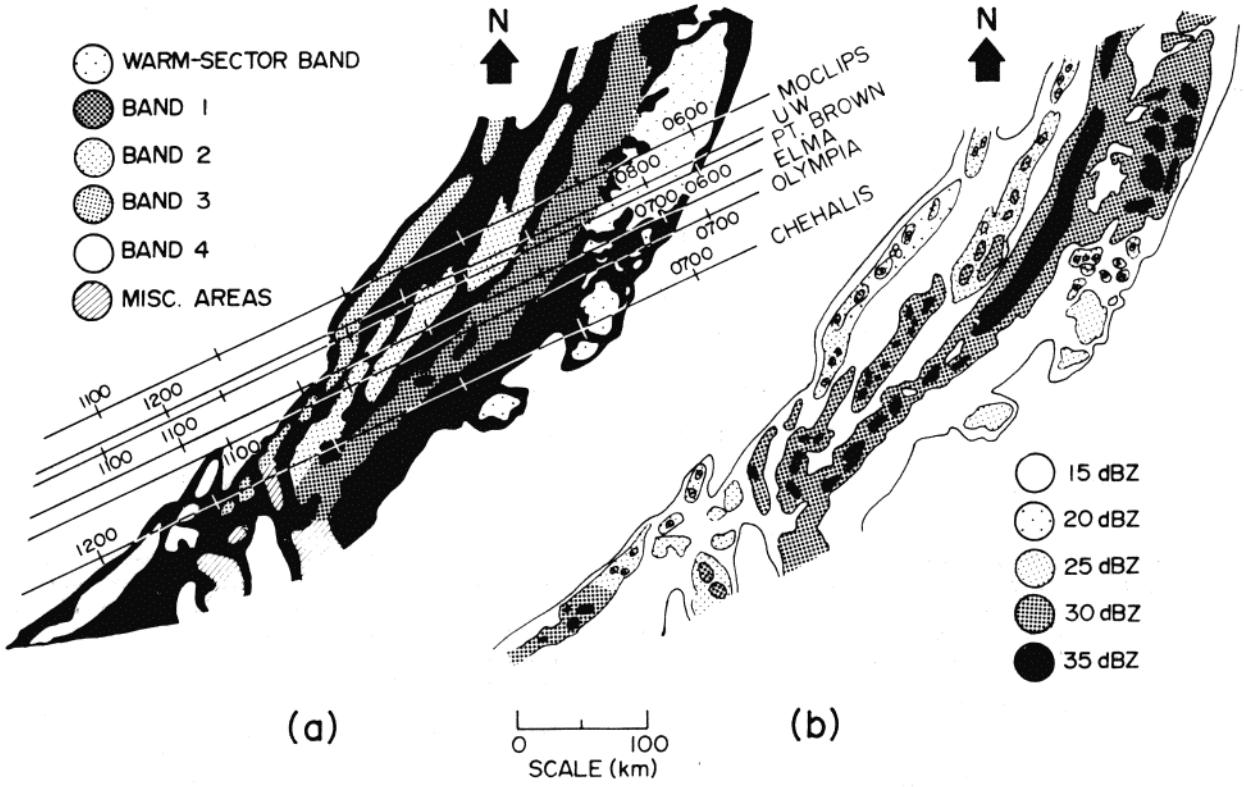

Figure 2. (a) Composite horizontal radar reflectivity pattern showing the warm-sector band and the sub-structure of the cold-frontal precipitation zone over Western Washington on November 17, 1976. The paths of the system over the six high-resolution precipitation gauges (whose locations are shown in Fig. 1) are indicated by the six straight lines. Shown on each line are the times that various portions of the system were over the given gauge. The precipitation rates at each of the gauges are shown in Fig. 3. (b) Reflectivity strengths of the rainbands shown in Fig. 2(a).

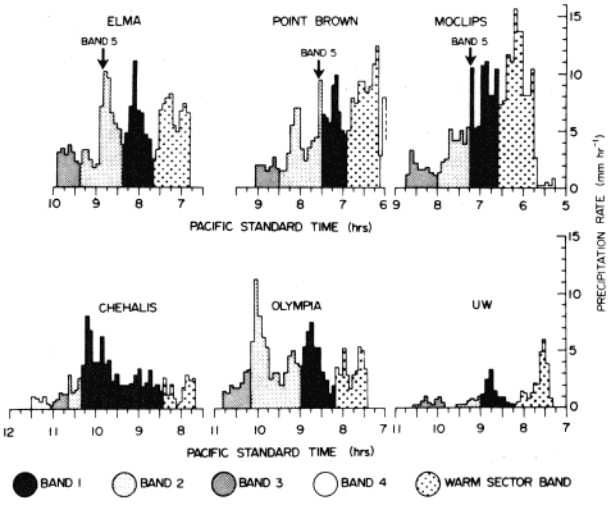

Figure 3. High-resolution precipitation rates at the six gauges shown in Figs. 1 and 2. The portion of the precipitation due to the warm-sector band and the bands associated with the cold-frontal zone are indicated by the same shading as in Fig. 2(a). The arrow shows the time that band 5 passed over each gauge.

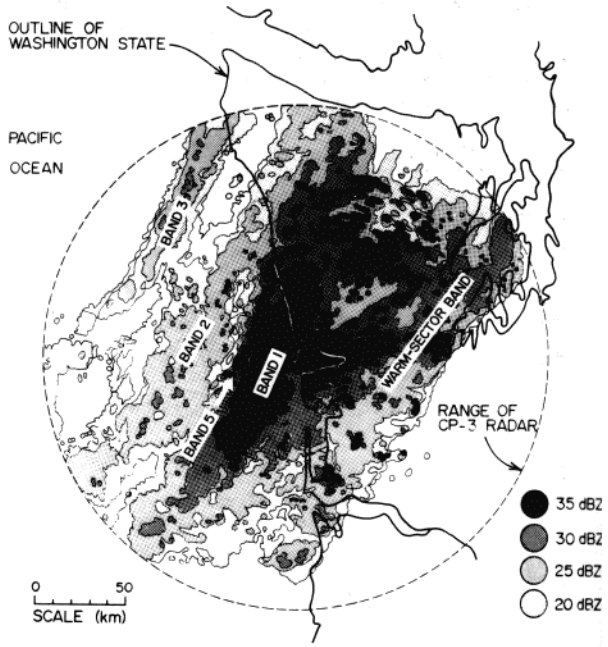

Figure 4. The horizontal radar reflectivity pattern at 0700 PST on November 17, 1976.

Some characteristics of the precipitation cores within rainbands 1-5 are listed in Table 1. Again, a distinction can be seen between the cores in bands 1-4 and those in band 5, namely, the cores in bands 1-4 moved, on average, toward 63° at a speed of 30 m s^{-1}, while those in band 5 moved toward 85° with a speed of 18 m s^{-1}.

In considering the motion of fronts or rainbands, two velocities may be used. The more informative is the complete velocity vector. However, to determine this the motion of at least one of the two end points of a front or a band has to be observed. When an end point is not observed, the velocity normal to the length of the front or rainband has to be used.

The vector velocities and the normal velocities for the cold-frontal precipitation zone, its embedded rainbands, the precipitation cores, and the upper-level cloud shield (determined from satellite images) are shown in Fig. 6. The

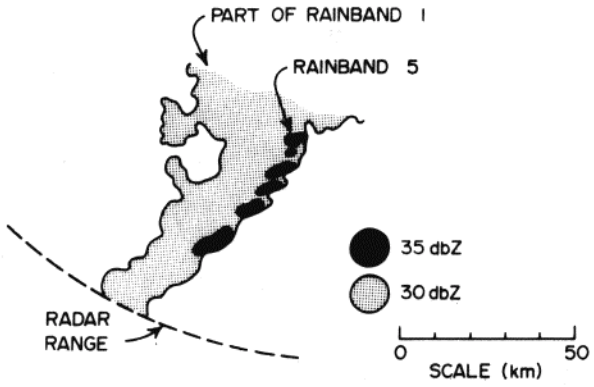

Figure 5. Part of the horizontal radar reflectivity pattern at 0822 PST showing the precipitation cores.

Table 1

Characteristics of the precipitation cores within the rainbands associated with the cold front

Rainband Number	Precipitation Cell Number	Area of Precipitation Core (km^2)	Speed of Precipitation Core ($m\ s^{-1}$)	Direction of Motion of Precipitation Core (*degrees*)	Time Tracked (*min*)
1	1	300	37	46	14
	2	64	32	64	16
	3	300	25	70	37
	Averages	200	31	60	
2	1	100	29	55	29
	2	60	18	60	20
	3	150	28	62	30
	4	150	29	66	50
	5	60	20	80	16
	6	150	27	70	15
	7	200	36	62	22
	8	60	30	65	45
	Averages	116	27	65	
3	1	40	37	64	28
	2	60	33	63	28
	3	40	27	66	15
	4	20	43	62	14
	5	80	42	64	15
	6	80	35	63	15
	7	220	35	55	15
	8	300	24	65	16
	9	80	34	60	38
	10	200	27	70	16
	11	50	34	64	38
3 (cont.)	12	200	38	68	14
	13	100	39	65	15
	Averages	113	34	64	
4	1	30	34	65	29
	2	30	30	62	15
	3	150	37	64	30
	4	25	27	64	15
	Averages	59	32	64	
5	1	25	22	90	14
	2	45	15	90	30
	3	100	12	90	112
	4	40	12	95	21
	5	25	14	90	22
	6	25	15	90	22
	7	200	15	85	29
	8	150	23	85	12
	9	10	20	80	15
	10	40	21	84	15
	11	40	19	80	31
	12	30	21	80	31
	13	16	18	85	31
	14	60	20	76	31
	15	64	20	82	15
	Averages	58	18	85	

accuracy of these velocity measurements is about ±2.5 m s^{-1}. It can be seen from Fig. 6 that the normal velocities of the cold-frontal precipitation zone, the surface frontal position, band 5 and its precipitation cores, and the upper-level cloud shield, were essentially the same. However, the normal velocities of bands 1-4 and their precipitation cores were significantly greater than the other features; consequently, bands 1-4 progressed through the frontal precipitation zone.

The maximum heights of the precipitation cores in the rainbands were determined from three-dimensional radar observations. The results are shown in Table 2, where it can be seen that the tops of the precipitation cores in bands 1-3 were about 5 and 6 km, while band 5 had tops between 1.5 and 4.5 km.

We turn now to the relationships between the horizontal winds and the motions of the

Table 2
Maximum heights of the precipitation cores in the rainbands associated with the cold front

Rainband Number	Maximum Height of Precipitation Cores (*km*)
1	6.1
2	5
3	5
4	---
5	1.5 - 4.5*

*Maximum height was somewhere between the two radar scan heights listed.

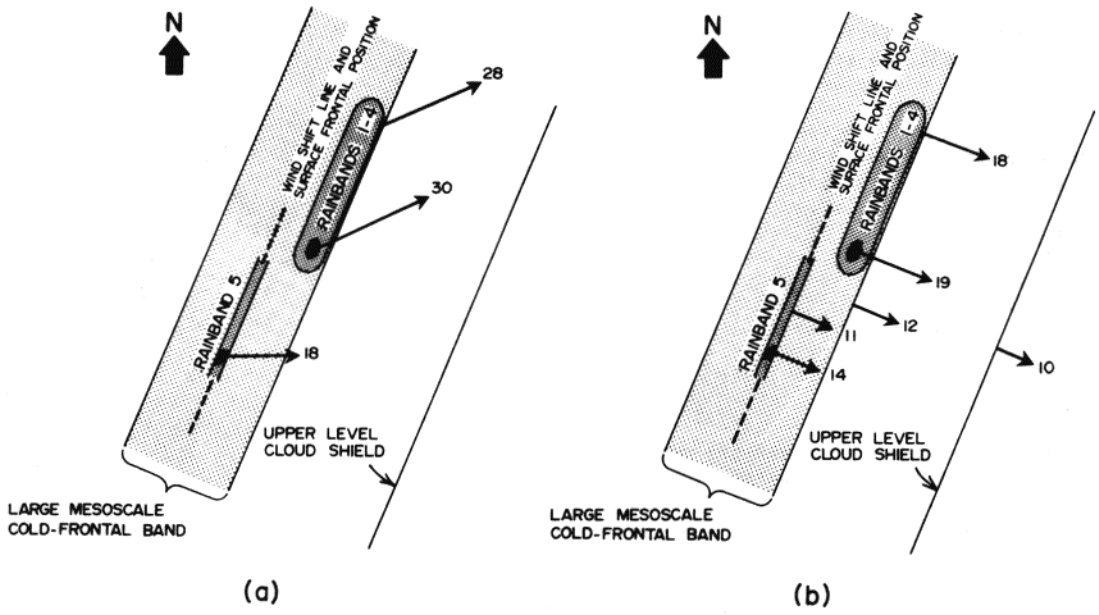

Figure 6. (a) Velocity vectors in m s^{-1} of the various components of the cold-frontal precipitation zone. (b) Velocities of the various components normal to the cold front. The smallest heaviest shaded components represent typical precipitation cores.

rainbands and their precipitation cores. Fig. 7 is a cross-section of the frontal system, through Pt. Brown, showing the wind directions deduced by the technique described by Locatelli and Hobbs (1978). Also shown are the wind directions and speeds from four rawinsondes launched from Pt. Brown during the passage of the system, the boundary of the precipitation particles detected by the radar, the locations of the rainbands deduced from the radar reflectivity data, and the location of the cold front at 1715 PST (15 min before it passed through Pt. Brown at the surface).

It can be seen from Fig. 7 that there was cold advection behind the front, as indicated by the backing of the winds with height, and that the main windshifts occurred in the lowest kilometer with the largest windshift at the surface. At the leading edge of the system was an overhang about 1 km thick which extended about 30 km ahead of the main body of the system. This overhang was due to "blow-off" from the warm-sector band. There was also an overhang, about 5 km thick, which extended some 90 km behind the main body of the frontal system and from which precipitation was falling and evaporating before reaching the surface.

The velocities of rainbands 1-4 and their precipitation cores (about 29 m s^{-1} or 56 knots toward 64° - see Fig. 6) are similar to the velocoties of the winds between about 3 and 6 km in altitude (Fig. 7). We conclude that these rainbands

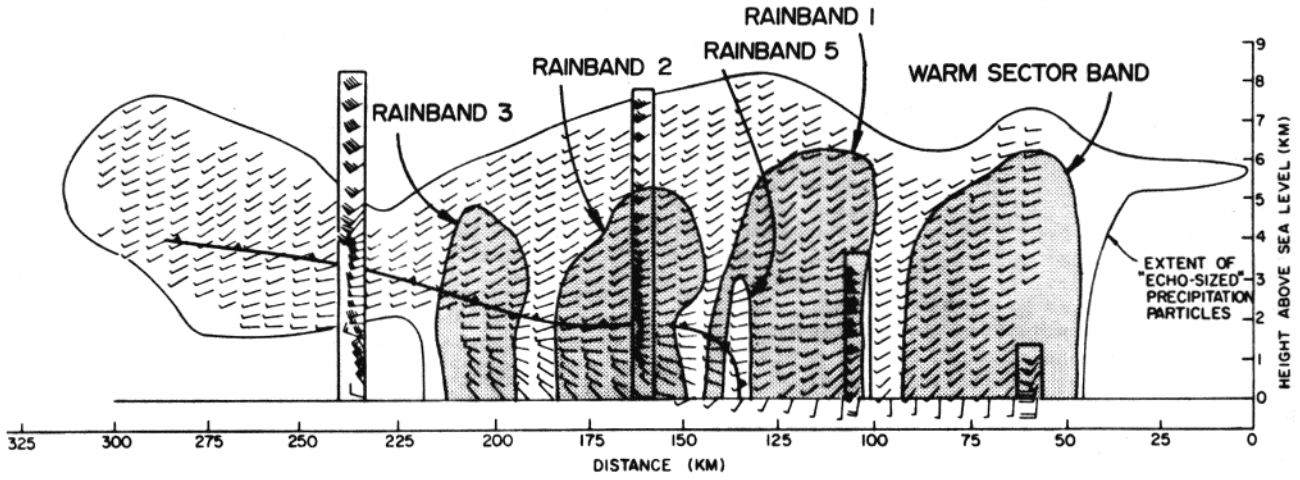

Figure 7. Cross-section of the frontal system through Pt. Brown on November 17, 1976. The detailed horizontal wind field (shown by the small arrows which indicate wind directions) was derived from Doppler radar measurements. Serial rawinsonde measurements (showing wind directions and speed in knots using conventional symbols) are plotted within the rectangular boxes. The warm-sector band, the rainbands associated with the cold-frontal zone, and the position of the front (at 0715 PST) are also shown.

were steered by the winds between 3 and 6 km, that is, near their upper levels.

The velocity of the precipitation cores in rainband 5 is 18 m s^{-1} or 35 knots toward 85° (see Fig. 6). The only location within the system where the winds have this velocity is in the vicinity of rainband 5 (see Fig. 7). Hence, unlike bands 1-4, rainband 5 was not steered by upper-level winds.

5. AIRFLOW WITHIN THE COLD-FRONTAL ZONE AND THE ORIGINS OF THE RAINBANDS

The flow of air within the cold-frontal precipitation zone was investigated by applying the equation of continuity to the horizontal components of the measured Doppler velocities in a vertical plane oriented perpendicular to the front. Vertical velocities of the air were calculated by assuming that no significant divergence occurred along the front and integrating the cross-front divergence upward in one-third-kilometer steps from the surface, where a vertical velocity of zero was assumed. Further details of the technique have been given by Matejka and Houze (1978).

Fig. 8 shows the derived streamflow *relative to the front* and the locations of the front and the rainbands relative to the streamflow. It can be seen that air in a shallow boundary layer ahead of the front moved toward the front in a relative sense. (The actual wind near the surface was south-southwest, almost parallel to the length of the front, and formed a low-level, moist, southerly jet - Fig. 7). Strong cross-front convergence (1.9 x 10^{-3} s^{-1}) occurred within 1 km of the surface, and air rose sharply with a vertical velocity of 1 m s^{-1} in a colume about 4 km in width at the center of band 5. This upward motion, originating close to the surface and centered on the front, no doubt produced rainband 5. When the rising column of air reached 3 km it encountered much stronger winds from the west (Fig. 7), and the updraft air was carried off to the east relative to the front (Fig. 8).

The precipitation efficiency in rainband 5 was approximately 25 per cent with respect to the flux of water vapor into its base and about 50 per cent with respect to the water which condensed within it.

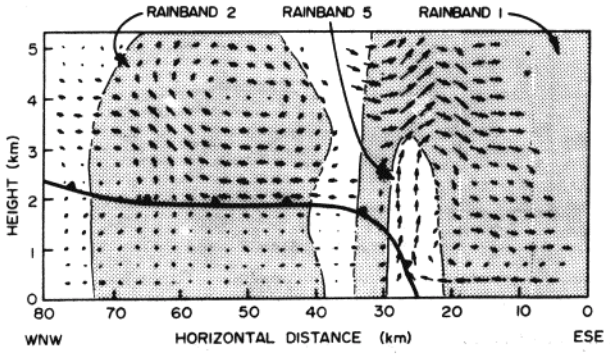

Figure 8. Cross-section through the cold-frontal band showing the streamflow relative to the front. The arrows represent five-minute displacements. The positions of the rainbands and the cold front are also shown.

A downdraft of about 0.5 m s^{-1}, and 4-5 km in width, was present between about 3 and 1.5 km in altitude just ahead of the updraft region discussed above. At the base of this updraft, was a region of strong divergence (1.1 x 10^{-3} s^{-1}).

Another region of fairly strong ascent, produced by horizontal convergence along the upper-level cold front, can be seen at altitudes from about 2.5 and 5 km at about 60 km on the horizontal scale in Fig. 8. This updraft lies within rainband 2 and coincides closely with the steering level for this band. It seems likely that the origins of the precipitation cores in band 2 (and, by analogy, in rainbands 1, 3 and 4) were associated with generating cells triggered by this upper-level convection. Hobbs and Locatelli (1978) have shown that precipitation cores in warm-frontal rainbands also originate in upper-level generating cells. By contrast, the cores in band 5, which was located on and moved with the cold front at the surface, originated in low-level convection.

6. AIRBORNE MEASUREMENTS

Extensive airborne measurements were obtained, from the University of Washington's (UW) B-23 and NCAR's Sabreliner aircraft, at various levels throughout the complete precipitation zone associated with the cold front. So far only a preliminary analysis has been made of the data from the B-23 aircraft, which flew in the lower regions of the frontal system. Consequently, we can only give a very sketchy picture of the microstructure of the system at this time; a detailed description will be given in a future publication.

Figure 9 shows the flight track of the B-23 aircraft through the complete precipitation zone (including the warm-sector and cold-frontal bands) associated with the cold front. Since this precipitation zone was changing as the aircraft traversed back and forth through it, the flight track has been divided into four legs (A-B, B-C, D-E and E-F). During each of these legs, the shape of the precipitation zone, as detected by the radar, did not vary greatly.

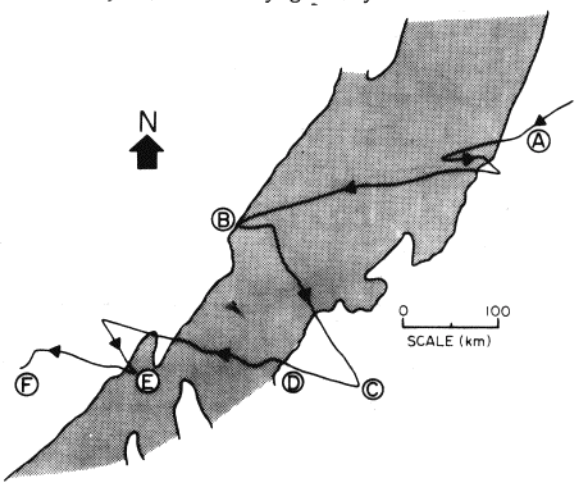

Figure 9. Flight tracks of the U.W.'s Cloud Physics research aircraft. Letters show the sections of the flight track depicted in Fig. 10. Shaded area shows the precipitation zone associated with the cold front (internal bands are not depicted).

Figure 10 shows vertical cross-sections through the four flight legs on which 1-minute average values (which correspond to a horizontal distance of about 3.9 km) of cloud liquid water contents (measured by the Johnson-Williams), ice particle concentrations (measured by the UW's Optical Ice Particle Counter) and air temperatures are plotted. These measurements show that there were only occasional patches of cloud liquid water (0.1-0.2 g m^{-3}) just above the melting level. (The values of 0.2-0.5 g m^{-3} at the end of flight leg B-C were not associated with the front but with orographic clouds over the western slopes of the Cascade Mountains.) However, the ice particle concentrations were generally in the range 1-10 ℓ^{-1}, with occasional patches of 1 ℓ^{-1} and some larger areas of 10-50 ℓ^{-1}. In the "overhang" at the rear of the system (legs D-E and E-F), the ice particle concentrations fell below 1 ℓ^{-1}. These concentrations are not unduly high when compared to the concentrations of ice nuclei which would be expected to be active at cloud top temperatures. The occurrence of ice particles in concentrations greater than 1 ℓ^{-1} is characteristic of clouds in mesoscale rainbands in extratropical cyclones (Matejka *et al.*, 1978).

7. SUMMARY

Fig. 11 summarizes our present picture of the mesoscale structure of the cold front discussed in this paper. Shown in this figure are five cross-sections (along approximately an east-west line) through the frontal system. The precipitation zone associated with the front contained within it six mesoscale rainbands: a warm-sector band, ahead of the front, four wide cold-frontal bands, and a narrow cold-frontal band. With the exception of the narrow cold-frontal band, the rainbands, and the precipitation cores within them, moved with the velocity of the winds in their upper levels. In the case of the wide cold-frontal bands, we have attributed this to the role of upper-level generating cells in triggering the precipitation. In contrast, the narrow cold-frontal band, which coincided with the surface frontal position, originated in low-level convection on the front, therefore, the velocity of this band was similar to that of the winds at the lower levels. The boundary-layer convection on the cold front was a consequence of the convergence of air in this region, produced by the front progressively overtaking a southerly jet of warm, moist air just ahead of the front.

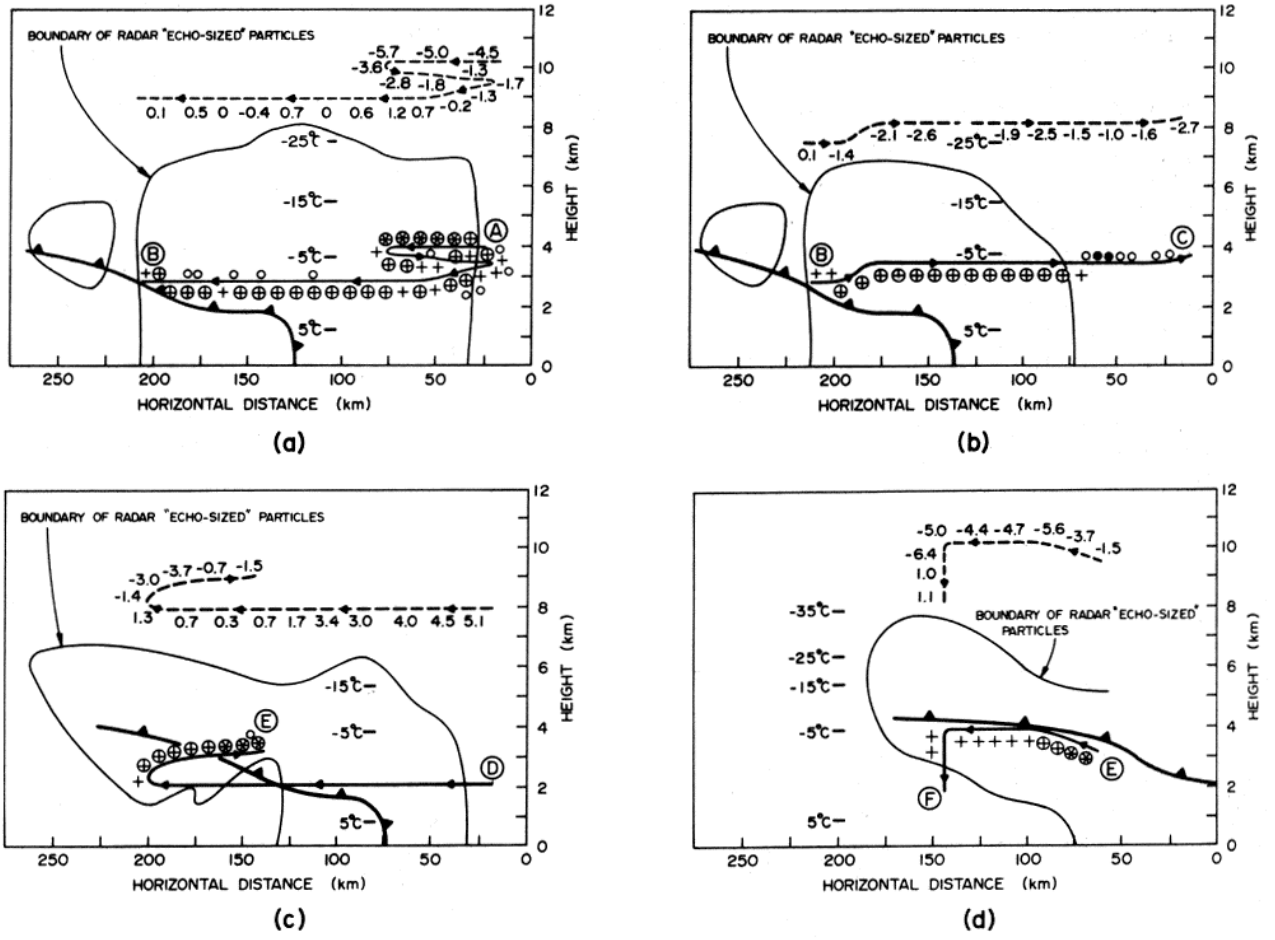

Figure 10. Vertical cross-sections through the precipitation zone associated with the cold front along flight legs (a) A-B, (b) B-C, (c) D-E and (d) E-F in Fig. 9. One-minute (3.9 km) average values of cloud liquid water content are indicated by: o - 0.1 to 0.2 g m^{-3}, ● - 0.2 to 0.5 g m^{-3}, and one-minute (3.9 km) average values of ice particle concentrations by: + - <1 ℓ^{-1}, ⊕ - 1 to 10 ℓ^{-1} and ⊗ - 10 to 50 ℓ^{-1}. Air temperatures (in °C) at flight level are plotted at the top of each diagram along the (displaced) dotted shape of the flight paths.

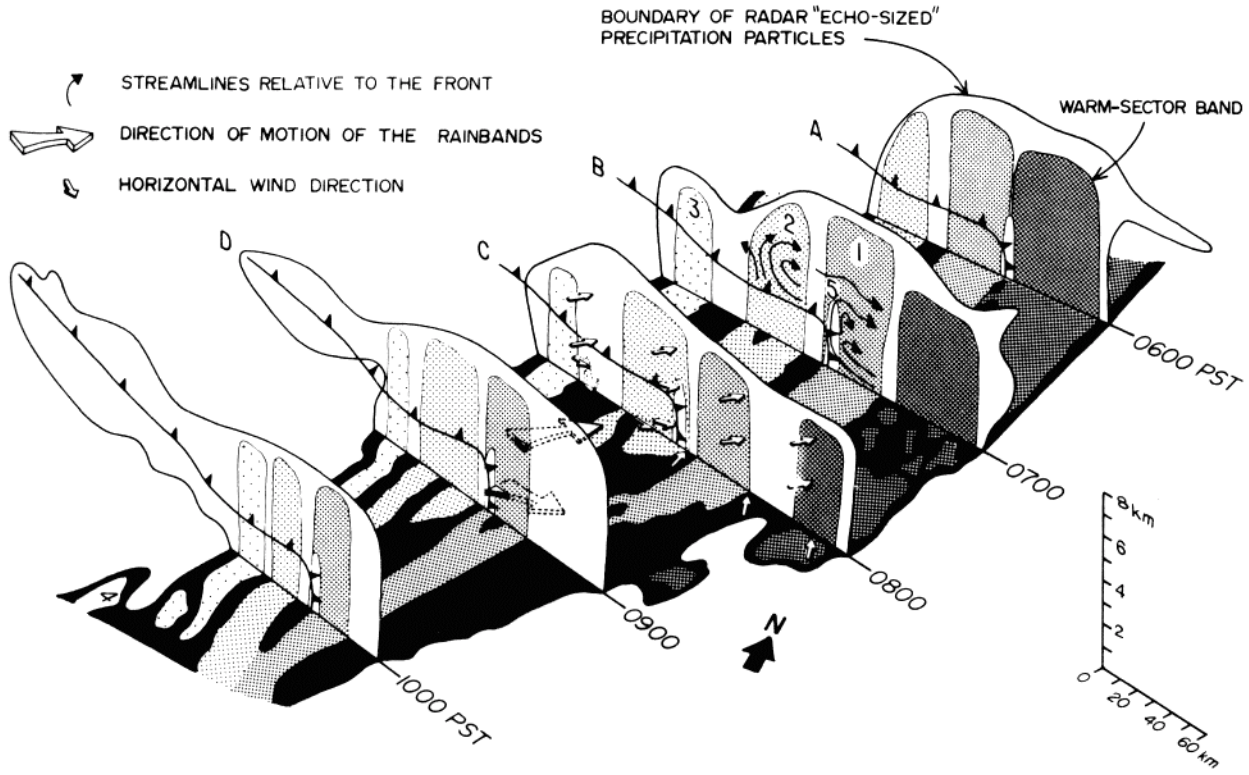

Figure 11. A schematic summary of the structure of the cold-frontal precipitation zone discussed in this paper.

Airborne measurements through the frontal system showed that the clouds consisted mainly of ice particles in concentrations of about 1 to 50 ℓ^{-1} with only occasional patches (0.1-0.2 g m^{-3}) of liquid water.

Acknowledgments. The CYCLES PROJECT is supported by the Atmospheric Research Section of the National Science Foundation (Grants ATM74-14726-A02 and ATM77-01344), the Air Force Office of Scientific Research (Contract F49620-77-C-0057), and the Environmental Research Laboratories of the National Oceanic and Atmospheric Administration (Grants 04-7-022-44023 and 44033). The CP-3 radar and Sabreliner were provided by the National Center for Atmospheric Research which is sponsored by the National Science Foundation. Thanks are due to all members of the Cloud Physics Group for their dedicated efforts in this Project.

REFERENCES

Austin, P. M., and R. A. Houze, Jr., 1972: Analysis of the structure of precipitation patterns in New England. J. Appl. Meteor. 11, 926-925.

Browning, K. A., and T. W. Harrold, 1969: Air motion and precipitation growth in a wave depression. Quart. J. Roy. Meteor. Soc., 95, 288-309.

Hobbs, P. V., 1978: The University of Washington's CYCLES PROJECT: an overview. Preprint Volume, AMS Conference on Cloud Physics and Atmospheric Electricity, Issaquah, Wn. (These Proceedings.)

Hobbs, P. V., and J. D. Locatelli, 1978: Rainbands, precipitation cores and generating cells in a cyclonic storm. J. Atmos. Sci., 35. (In press.)

Locatelli, J. D., and P. V. Hobbs, 1978: A technique for obtaining detailed wind fields in a frontal system from a single Doppler radar. J. Appl. Met. (In press.)

Matejka, T. J., and R. A. Houze, Jr., 1978: Doppler radar measurements of the airflow within a mesoscale cold-frontal rainband. Preprint Volume, 18th AMS Conference on Radar Meteorology, Atlanta, Ga., 17-22.

_____, _____, and P. V. Hobbs, 1978: Microphysical and dynamical structure of mesoscale cloud features in extratropical cyclones. Preprint Volume, AMS Conference on Cloud Physics and Atmospheric Electricity, Issaquah, Wn. (These Proceedings.)